
This is an electronic reprint of the original article.
This reprint may differ from the original in pagination and typographic detail.

Sathyan, Sabin; Aydin, Ugur; Lehtikoinen, Antti; Belahcen, Anouar; Vaimann, Toomas; Kataja, Juhani

Influence of magnetic forces and magnetostriction on the vibration behavior of an induction motor

Published in:
International Journal of Applied Electromagnetics and Mechanics

DOI:
[10.3233/JAE-171045](https://doi.org/10.3233/JAE-171045)

Published: 01/01/2019

Document Version
Peer-reviewed accepted author manuscript, also known as Final accepted manuscript or Post-print

Please cite the original version:
Sathyan, S., Aydin, U., Lehtikoinen, A., Belahcen, A., Vaimann, T., & Kataja, J. (2019). Influence of magnetic forces and magnetostriction on the vibration behavior of an induction motor. *International Journal of Applied Electromagnetics and Mechanics*, 59(3), 825-834. <https://doi.org/10.3233/JAE-171045>

This material is protected by copyright and other intellectual property rights, and duplication or sale of all or part of any of the repository collections is not permitted, except that material may be duplicated by you for your research use or educational purposes in electronic or print form. You must obtain permission for any other use. Electronic or print copies may not be offered, whether for sale or otherwise to anyone who is not an authorised user.

Influence of Magnetic Forces and Magnetostriction on the Vibration behavior of an Induction Motor

Sabin Sathyan^a, Ugur Aydin^a, Antti Lehtikoinen^a, Anouar Belahcen^{a, b}, Toomas Vaimann^b and Juhani Kataja^c

^a *Aalto University, Dept. of Electrical Engineering and Automation, PO Box 15500, FI-00076, Finland*

^b *Tallinn University of Technology, Dept. of Electrical Power Engineering and Mechatronics, 19086 Tallinn, Estonia*

^c *CSC-IT Center for Science, PO Box 405, FIN-02101, Espoo, Finland*

Abstract. This paper presents the vibration analysis and results of an induction motor through two kinds of magneto-mechanical coupling methods. The computation results are validated by comparing them with the vibration measurements of the motor. The role of both the magnetic forces and magnetostriction are examined and distinguished based on their contribution to the vibration behavior of the machine. It was found that the pole pair number of an induction machine can affect the way the vibrations caused by magnetostriction and magnetic forces either add up or oppose each other.

Keywords: Finite element analysis, magnetic forces, magnetostriction, magnetomechanical coupling

1. Introduction

The electromagnetic causes of stator vibrations occurring in induction motors are known to be magnetic forces and magnetostriction (MS) [1]. While these two phenomena cause deformation in the stator core and thereby produce vibrations and acoustic noise, the combined role of magnetic forces and magnetostriction can vary in different machines. Because the effects of the magnetic forces and magnetostriction can either add up or get subtracted, it affects the amount of deformation and vibrations differently. In this paper, the stator vibrations of an induction motor are measured and compared with the simulation results of two methods. The first one is a directly coupled system of equations where the nodal magnetic forces are fed to the elasticity solver to get the displacements. The second one is a magneto-mechanical system of equations, which takes into account magnetostriction.

The computation of magnetic forces can be done by means of different methods such as the Maxwell stress tensor [2] and the virtual work principle [3-5]. In this paper, both the Maxwell stress tensor and local application of the principle of the virtual work are employed. Magnetostriction causes strains in ferromagnetic materials in the presence of magnetic fields. This phenomenon couples elastic and magnetic fields in magnetic materials. The deformation in ferromagnetic materials due to MS is attributed to the rotation of magnetic domains, which are randomly oriented when the material is not under the influence of a magnetic field. With an externally applied magnetic field, the domains orient themselves to align with the magnetic field in every region, which creates a magnetostrictive strain field. In this paper, the magneto-mechanical coupling including MS is performed by making use of the Helmholtz free energy density [6], which is defined as a function of five scalar invariants, and the anhyseretic mechanical behavior is obtained by minimizing this energy. This method has been studied and further developed in various researches. For example, in [7], this model is extended to include magnetic hysteresis, and in [8, 9], the coupling in electrical steel sheets under biaxial and multiaxial stress is presented using the same model.

The role of magnetic forces and MS in motor vibrations were studied by different researchers, where the results have shown that the interaction of these two phenomena can either escalate or attenuate stator vibrations [6, 10, 11]. In this study, it has been verified in a four pole and a two pole induction motor using magneto-mechanical coupled models in finite element analysis. The simulated results were used for frequency analysis. The computed and measured frequency components in vibrations are compared and recognized to be identical.

2. Computational methodology

2.1. Nodal magnetic forces and magneto-elastic coupling

The generalized nodal forces are computed by locally differentiating the magnetic energy W_s with respect to a virtual displacement s :

$$\mathbf{F} = \frac{-\partial W_s}{\partial s} = \int_V \nu \mathbf{B} \cdot \mathbf{u} \nabla N \cdot \mathbf{B} - \frac{\nu}{2} \mathbf{u} \cdot \nabla N \mathbf{B}^2 dV$$

where ν is the magnetic reluctivity of the medium, \mathbf{B} the magnetic flux density, \mathbf{u} is the unit vector in the displacement direction and N the finite element nodal shape function.

The deformation in electrical machines is analyzed as a linear elasticity problem using Navier equations. The dynamic equations for elastic deformation of solids is

$$\rho \frac{\partial^2 \mathbf{d}}{\partial t^2} - \nabla \cdot \boldsymbol{\tau} = \mathbf{f}$$

where ρ is the mass density, \mathbf{d} is displacement field, \mathbf{f} the given body force and $\boldsymbol{\tau}$ the stress tensor. The magneto-elastic model is implemented in the open-source software *Elmer* and is simulated hierarchically, first solving the magnetic system and then providing the elasticity solver with the magnetic nodal forces as the volume force on the right side of (2).

2.2. Energy based magneto-mechanical model

In order to couple the magnetic and elastic properties of the material, the constitutive equations are formulated from a Helmholtz free energy density ψ [6-9]. For an isotropic magneto-elastic material, ψ is expressed as a function of five scalar invariants, which depend on the magnetic flux density vector \mathbf{B} and total strain tensor $\boldsymbol{\varepsilon}$:

$$I_1 = \text{tr}(\boldsymbol{\varepsilon}), \quad I_2 = \frac{1}{2} \text{tr}(\boldsymbol{\varepsilon}^2), \quad I_4 = \frac{\mathbf{B} \cdot \mathbf{B}}{\mathbf{B}_{\text{ref}}^2}, \quad I_5 = \frac{\mathbf{B} \cdot (\tilde{\boldsymbol{\varepsilon}} \mathbf{B})}{\mathbf{B}_{\text{ref}}^2}, \quad I_6 = \frac{\mathbf{B} \cdot (\tilde{\boldsymbol{\varepsilon}}^2 \mathbf{B})}{\mathbf{B}_{\text{ref}}^2}$$

where $\mathbf{B}_{\text{ref}} = 1$ T. The first three invariants describe the elastic behavior of the material, and I_3 (not defined here) is not used, as linear elasticity is assumed. The fourth invariant corresponds to the single-valued magnetization behavior and the fifth and sixth invariants determine the magneto-elastic coupling. Since the permeability variation is independent of the hydrostatic pressure, in the fifth and sixth invariants, the deviatoric part of the strain $\tilde{\boldsymbol{\varepsilon}} = \boldsymbol{\varepsilon} - \varepsilon_{\text{Hyd}}$ is used, where ε_{Hyd} is the hydrostatic strain. The expression for the Helmholtz free energy density is then given as

$$\psi = \frac{1}{2} \lambda I_1^2 + 2G I_2 - \nu_0 \left(\frac{I_4}{2} + \sum_{i=0}^{n_\alpha-1} \frac{\alpha_i}{i+1} I_4^{i+1} + \sum_{i=0}^{n_\beta-1} \frac{\beta_i}{i+1} I_5^{i+1} + \sum_{i=0}^{n_\gamma-1} \frac{\gamma_i}{i+1} I_6^{i+1} \right)$$

Here, λ and G are the Lamé constants of the material, ν_0 is the reluctivity of free space and $\alpha_i, \beta_i, \gamma_i$ are the fitting parameters to be identified from measurements. The magneto-elastic stress and magnetization are obtained as

$$\boldsymbol{\sigma}_{me}(\mathbf{B}, \boldsymbol{\varepsilon}) = \frac{\partial \psi(\mathbf{B}, \boldsymbol{\varepsilon})}{\partial \boldsymbol{\varepsilon}} \quad \text{and} \quad \mathbf{M}(\mathbf{B}, \boldsymbol{\varepsilon}) = - \frac{\partial \psi(\mathbf{B}, \boldsymbol{\varepsilon})}{\partial \mathbf{B}}$$

The magnetic field strength vector is $\mathbf{H} = \nu_0 \mathbf{B} - \mathbf{M}$. The magneto-elastic stress tensor $\boldsymbol{\sigma}_{me}$ consists of elastic and magnetostriction related stress tensors.

Fifteen parameters were needed to model the properties of the studied material (0.5 mm non-oriented Si-Fe sheets) and they were determined using the experimental data obtained from a custom-built uniaxial single sheet tester [12]. In the experimental process, the material was loaded with different stresses varying from 50 MPa compression (-) to 80 MPa tension (+) parallel to the flux density, and the magnetization curves were measured. Afterward, initial fitting of the single-valued model parameters to the H -averaged measured magnetization loops was realized at various stress values, as shown in Fig. 1. Magnetic materials show reduced permeability under compression and high tension. This behavior of magnetic materials is modeled successfully using the model. Besides, increased permeability is observed under low tensile stress as reported in [12].

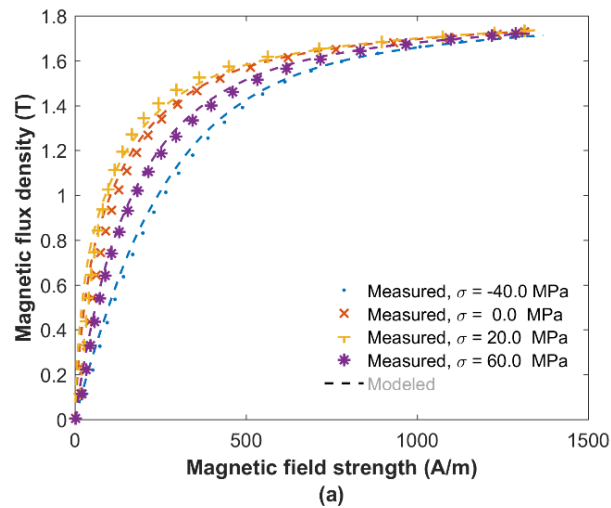


Fig. 1. Fitting results of the single-valued model parameters with H -averaged magnetization curve measurements

The magnetomechanical problem was solved with the finite element method implemented in Matlab. First-order shape functions were used for both the vector potential and the displacements. All field and circuit quantities were strongly coupled. Rotor motion was taken into account with the moving band approach [13], and the same air-gap mesh was used to evaluate the Maxwell stress tensor in the air-gap.

3. Vibration measurements

The machine under investigation (specifications in Table 1) was supplied by an autotransformer and loaded by an identical machine fed from a frequency converter to ensure for different loading levels correctly. The coupling between the two machines is well balanced in order to avoid any unwanted effects from the loading machine to the measured machine's vibrations. Five triaxial accelerometers corresponding to 15 vibration channels are distributed around the machine frame as given in Fig. 2. For vibration sensor installation, three different axial positions were prepared for testing and flat surfaces were machined to the motor shell, as shown in Fig. 2. The x , y and z axes measure radial, tangential and axial vibrations respectively. The measured signals were recorded by a digital multi-channel recorder and stored in the computer. All the channels are fully synchronized with a sampling frequency of 10 kHz. The schematic diagram of measurement set up is shown in Fig. 3. The influence of the PWM drive of the loading machine is not explored in this study, although this could have minor effects on some vibration frequencies in the spectra of tested machine.

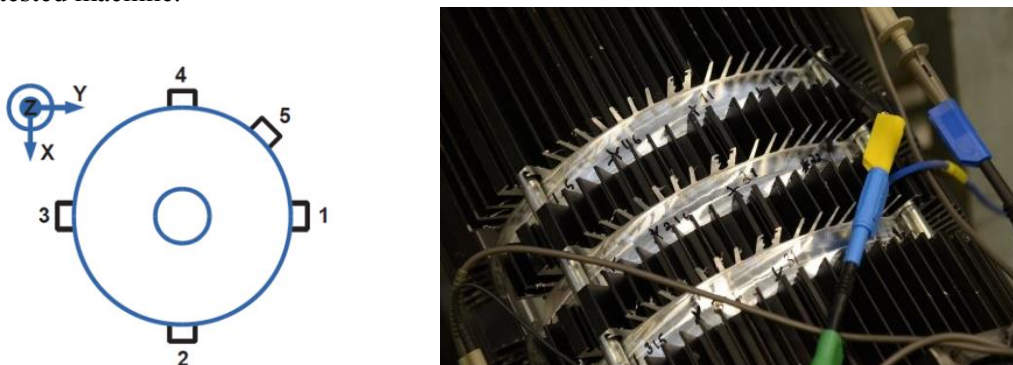


Fig. 2. The position of accelerometers around the stator frame (left) and flat surface on motor shell for sensor mounting (right)

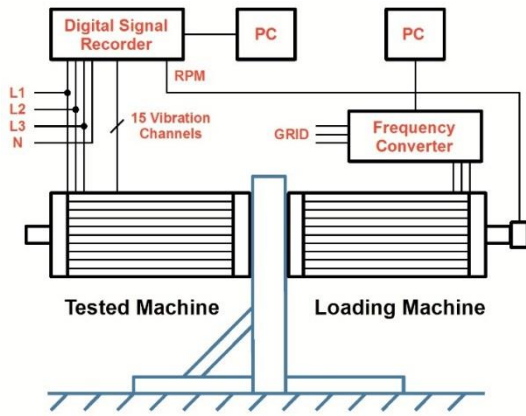


Fig. 3. Schematic of Measurement set up

Table 1	
Specifications of the motor under investigation	
Parameter	Value
Number of poles	4
Number of phases	3
Connection	Star
Terminal voltage	415V@60 Hz; 325V@50 Hz
Rated slip	0.06
Rated power	22kW@60 Hz; 18kW@50 Hz
Stack length	0.23m

4. Results and discussions

4.1. Matlab simulations

The mesh and flux density distribution from Matlab simulation is shown in Fig. 4. The results are from time-stepping simulations with a simulation time of 0.6 sec (6000 time-steps) and has a timestep length of 0.0001 sec. The mesh has 694 nodes and 1162 triangular elements. In Fig. 5, the deformation of the motor in three different cases viz., due only to magnetic forces, due only to MS and due to both magnetic forces and MS are given. The magnetic forces contract the stator core, while the MS expands it. Two simulations were done for each case for radial and tangential displacements. The displacements of the outer nodes of the stator and inner nodes of the rotor were fixed to zero in tangential direction for radial displacement simulations and those were fixed in radial direction for the tangential displacement simulations.

The displacements at a point on the stator outer surface is compared in Fig. 6 and it is clearly seen that, the displacement due to magnetic forces and MS are opposite in phase and they oppose each other, and hence the final displacement gets attenuated. The use of first order triangular elements in mechanical simulation can cause locking effects and deformation of the mesh will be affected by this phenomenon. With the purpose of avoiding this consequence and to get a more accurate result, simulations were done using second order elements. The results are shown in Fig. 7. From the figure, it is clear that, the displacements are increased in the second order case, compared to the first order simulations.

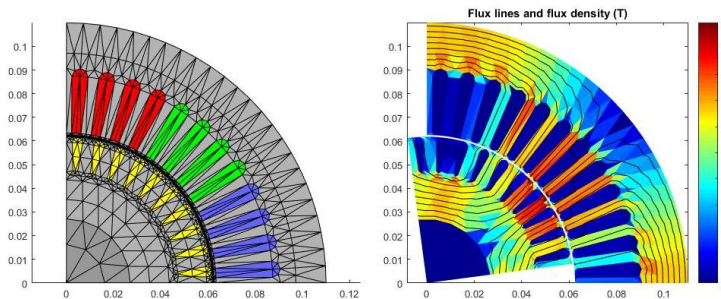


Fig. 4. Finite element mesh of the motor (left) and magnetic flux density distribution (right)

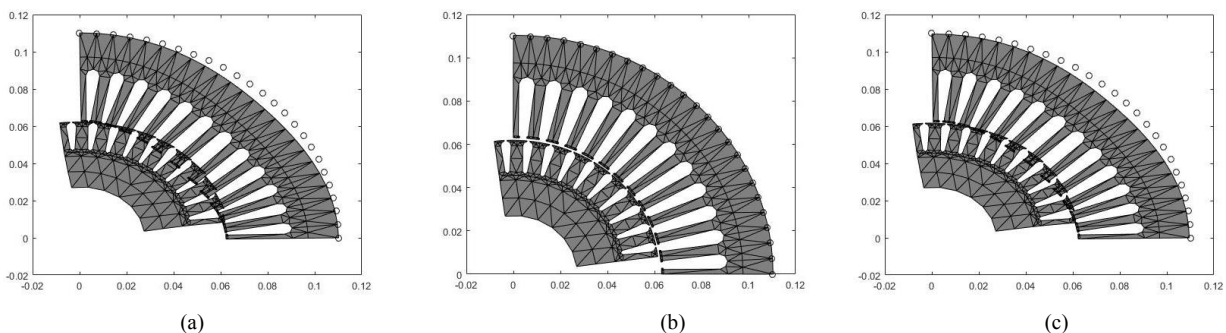


Fig. 5. Deformation of the four pole motor due to (a) magnetic forces only, (b) magnetostriction only and (c) both magnetic forces and magnetostriction. Displacement scale factor: $1e4$. The dotted line denotes the original stator outer boundary.

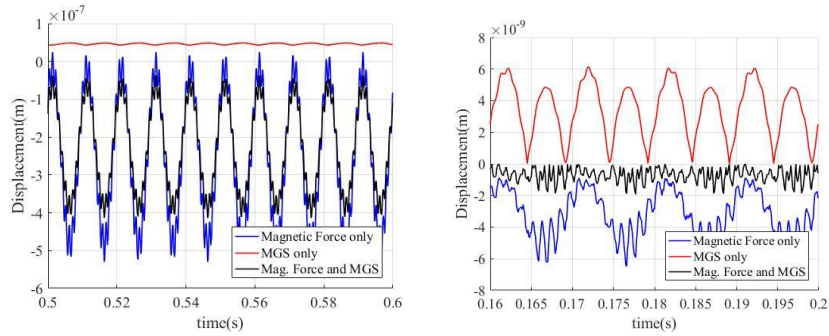


Fig. 6. Simulated displacements at a point on the stator outer surface of the four pole motor. Left: Radial displacements, Right: Tangential displacements.

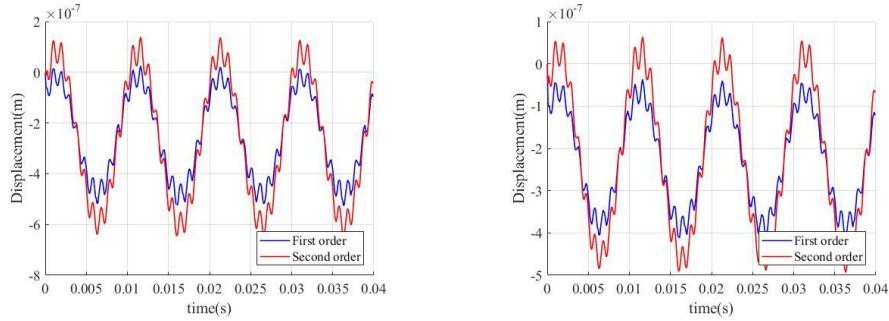


Fig. 7. Comparison of simulated radial displacements at a point on the stator outer surface of the four pole motor between first order and second order simulations. Left: Displacement due to only magnetic forces, Right: Displacement due to both magnetic forces and MS

In order to analyze the interaction of magnetic forces and MS in a two pole configuration, the same motor was simulated as a two pole motor. The displacement comparison of the two pole motor in Fig. 8 shows that, the magnetic forces and MS are in phase and the resulting displacement get strengthened, because the contribution of magnetic forces and MS add up in this case. The deformed mesh of the two pole motor in three different cases is shown in Fig. 9.

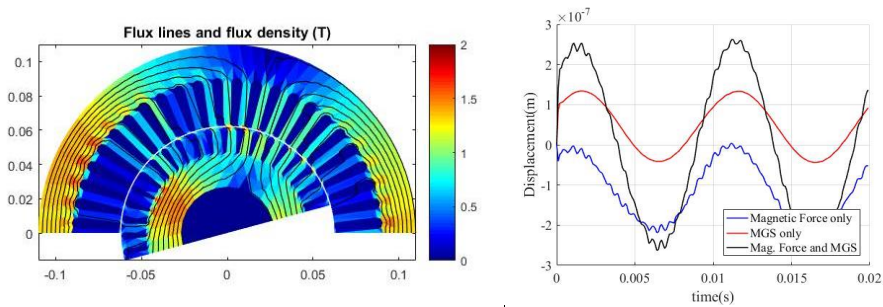


Fig. 8. Left: Flux density distribution at the two pole motor, Right: Simulated radial displacements at a point on the stator outer surface

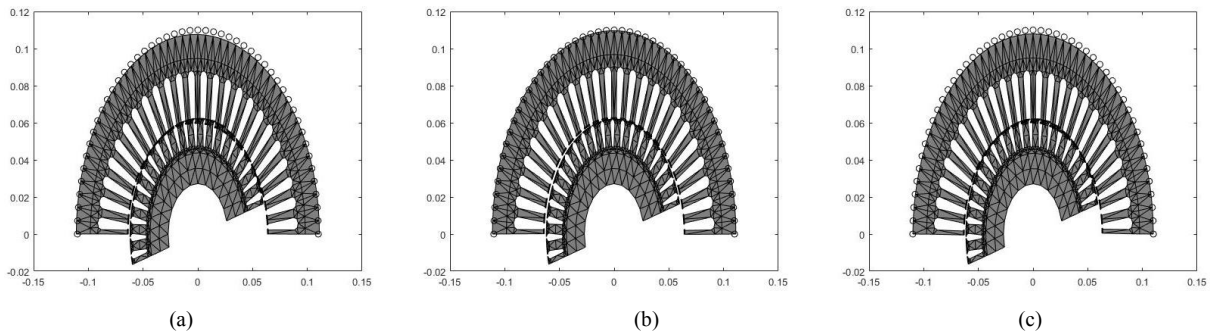


Fig. 9. Deformation of the two pole motor due to (a) magnetic forces only, (b) magnetostriction only and (c) both magnetic forces and magnetostriction. Displacement scale factor: $1e4$. The dotted line denotes the original stator outer boundary.

4.2. Elmer simulations

The simulations in *Elmer* were carried out to focus on the impact of nodal magnetic forces, which are computed using the virtual work principle. The time-stepping simulation had a total simulation time of 1.2 seconds (6000 time-steps) with 0.0002 seconds as a time-step length. The mesh contains 89892 elements and 45003 nodes. The nodal forces are majorly distributed on the stator teeth as shown in Fig. 10. The displacements at a point on stator surface calculated using the nodal forces as excitation in mechanical simulation is shown in Fig. 10 (c). This simulation also gives very similar result as in the Matlab where the Maxwell stress tensor is used for force calculation.

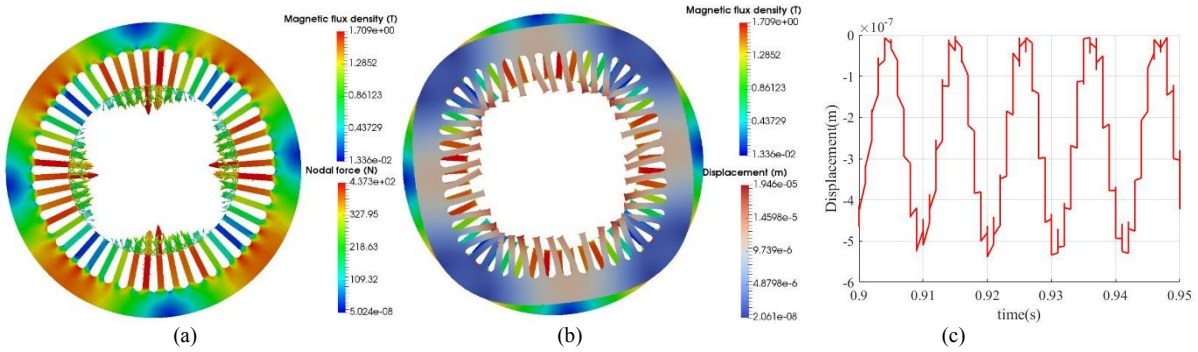


Fig. 10. *Elmer* simulation results. (a) Nodal forces on the stator teeth, (b) deformed stator compared to original (Displacement scale factor: 1e3), (c) radial displacements at a point on the stator outer surface due to nodal magnetic forces

4.3. Vibration frequency analysis – measurements and simulations

In this stage of the study, frequency analysis of the measured vibrations and simulated displacements were done in order to discover the major frequency components. The Fourier analysis results of measurement and simulations are given in Fig. 11 and Fig. 12 respectively. In the low frequency region, the main components present are the rotational speed frequency f_{ix} calculated by, $rotational\ speed / 60 = 1400/60 = 23.3\ Hz$ and the twice line frequency $2f_L$ (100 Hz) and its integer multiples. The rotor bar passing frequency (f_{QR}) due to the magnetic field around the rotor bars produced by rotor currents is given by, $f_{ix} * number\ of\ rotor\ slots = 932\ Hz$. The sidebands of f_{QR} at $\pm 2f_L, 4f_L, 6f_L$ and $8f_L$ correspond to 832 Hz, 1032 Hz, 732 Hz, 1132 Hz, 632 Hz, 1232 Hz, 532 Hz and 1332 Hz are also present. At 341 Hz in Fig. 11, relatively high magnitude of acceleration is seen in the frequency spectrum, which is caused by the structural vibration of the entire machine set up. It has to be noted that, comparison between measurement and simulation are concentrated only for the frequency components and comparison of magnitudes of the measured vibration spectra and calculated vibrations from the simulated displacements is problematic, as there will be considerable difference in the floor level of the spectrum. The acceleration corresponds to a displacement d and angular frequency $\omega = 2\pi f$ can be calculated by the formula $\omega^2 d$. The displacement corresponds to 100 Hz from the simulation result gives an acceleration of $0.005\ m/s^2$. The measurement vibration at 100 Hz is around $0.006\ m/s^2$.

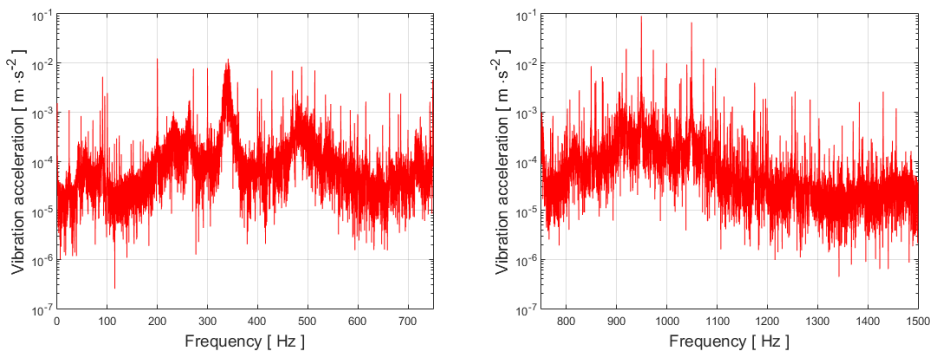


Fig. 11. Radial vibration frequency spectra from measurements

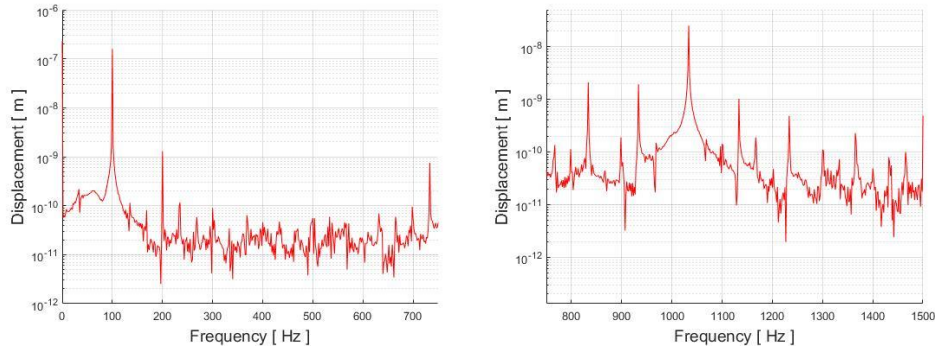


Fig. 12. Radial vibration frequency spectra from simulation

5. Conclusions

The results from the finite element studies using the magneto-mechanical coupled models reveal that, the effect of magnetic forces and MS can have varying influence on different kinds of machines, as they can either strengthen up or counteract each other and which affects the amount of deformation and vibrations contrarily. The influence of pole numbers in an induction motor is analyzed in this paper and studies need to be done for other types of machines to understand how magnetic forces and MS act in varied designs. Besides, the MS induced deformations show that, in magneto-mechanical studies of electrical motors such as stress and noise analysis, magnetostriction is an inexorable factor. The study also examined the vibration frequency spectra of the motor and the proposed magneto-mechanical models successfully modeled the spectra, which is an imperative aspect in noise analysis of electrical machines.

Acknowledgements

The authors thank TEKES (Finnish Funding Agency for Innovation) for their support under SEMTEC project Grant 5146/31/2014 and the European Research council for European Union's seventh framework programme (FP7/2007-2013)/ERC grant agreement n° 339380. This work was partly supported by the Estonian Research Council grants PUT 1260.

References

- [1] A. Belahcen, "Magnetoelasticity, magnetic forces and magnetostriction in electrical machines", doctoral thesis, Helsinki University of Technology, Lab. Of Electromechanics, report. 72, 2004, pp 23-32.
- [2] J. C. Coulomb, "A methodology for the determination of global electromechanical quantities from a finite element analysis and its application to the evaluation of magnetic forces, torques and stiffness", *IEEE Trans. mag.*, MAG-19, n.6, pp. 2514–2519, 1983.
- [3] A. Bossavit, "Edge-element computation of the force field in deformable bodies", *IEEE Trans.Mag.*, v.28, n.2, pp.1263-1266, 1992.
- [4] Z. Ren, A. Razek, "Local force computation in deformable bodies using edge elements", *IEEE Trans.Mag.*, v.28, n.2, pp. 1212–1215, 1992.
- [5] Kameari, A., "Local calculation of forces in 3D FEM with edge elements", *International Journal of Applied Electromagnetics in Materials*, Vol. 3, 1993, pp. 231–240.
- [6] K. Fonteyn, A. Belahcen, R. Kouhia, P. Rasilo, and A. Arkkio, "FEM for directly coupled magneto-mechanical phenomena in electrical machines," *IEEE Trans. Magn.*, vol. 46, no. 8, pp. 2923–2926, Aug. 2010.
- [7] P. Rasilo et al., "Modeling of hysteresis losses in ferromagnetic laminations under mechanical stress," *IEEE Trans. Magn.*, vol. 52, no. 3, Mar. 2016, Art. no. 7300204
- [8] U. Aydin, P. Rasilo, D. Singh, A. Lehikoinen, A. Belahcen, A. Arkkio, "Coupled magneto-mechanical analysis of iron sheets under biaxial stress", *IEEE Trans. Magn.*, vol. 52, no. 3, sequence no. 2000804, March 2016.
- [9] U. Aydin, P. Rasilo, F. Martin, D. Singh, L. Daniel, A. Belahcen, R. Kouhia, A. Arkkio, "Modelling the effect of multiaxial stress on magnetic hysteresis of electrical steel sheets: a comparison", *IEEE Trans. Magn.* Vol. 53, no. 6, sequence no. 2000904, June 2017.
- [10] T.G.D. Hilgert, L. Vandeveld, J.A.A. Melkebeek, "Numerical analysis of the contribution of magnetic forces and magnetostriction to the vibrations in induction machines", *IET Science. Meas. And Tech.*, v. 1, issue.1, pp. 21-24, Jan. 2007
- [11] L. Vandeveld et al, "Finite-element computation of the deformation of ferromagnetic material taking into account magnetic forces and magnetostriction". *IEEE. Trans. Magn.* Vol.40, issue.2, pp. 565-568, March 2004
- [12] D. Singh, P. Rasilo, F. Martin, A. Belahcen, and A. Arkkio, "Effect of mechanical stress on excess loss of electrical steel sheets," *IEEE Trans. Magn.*, vol. 51, no. 11, Nov. 2015, Art. ID 1001204.
- [13] B. Davat, Z. Ren, M. Lajoie-Mazenc, "The movement in the field modeling", *IEEE Trans. Magn.*, vol. 21, issue. 6, pp. 2296-2298, Nov. 1985